Metal-organic-framework transparency to water interactions for enhanced CO_2 adsorption

Aziz Ghoufi*

Institut de Physique de Rennes, IPR, CNRS-Université de Rennes 1, UMR CNRS 6251, 35042 Rennes, France and Univ Paris-East Creteil, CNRS, ICMPE (UMR 7182), 2 rue Henri Dunant, Thiais F-94320, France

(Received 14 July 2023; revised 31 August 2023; accepted 22 November 2023; published 20 December 2023)

Today, the capture of post-combustion CO_2 has become a global priority, particularly in order to curb rising temperatures in the coming decades. CO_2 physisorption in porous materials such as metal-organic frameworks is likely one of the most effective approaches to addressing this problem, thanks to its low energy requirement and improved regeneration process. In this study, I investigated CO_2 capture in humid conditions using the Al-MIL-53-TDC metal-organic framework through molecular simulations. I observed that water filling occurs gradually through pore capillary condensation. Remarkably, the presence of water (at a hydration rate of 4.4 wt%) resulted in a significant increase of 283% in the adsorbed amount of CO_2 (1.8 mmol/g at 0.2 bar) due to a unique transparency property. The thin molecular walls between the uniaxial channels enable van der Waals and electrostatic interactions between water and adsorbed gas, which allow media on opposite sides of the walls to influence each other. The increase in isosteric heat of adsorption (46 kJ/mol) is attributed to the contribution of water/water energy resulting from the truncation of the hydration shell of water. This truncation increases the number of hydrogen bonds, which can be linked to a kosmotropic effect. Additionally, the selectivity of hydrated Al-MIL-53-TDC for CO_2/N_2 increased by 185% at 0.2 bar (composition 20:80), compared to the unhydrated MOF material with QsT $<$ 50 kJ/mol.

DOI: 10.1103/PhysRevMaterials.7.126001

I. INTRODUCTION

In 2022, global CO_2 emissions remained at record levels, with no indication of the urgent reduction necessary to achieve the Paris agreement's most ambitious target of limiting global warming to 1.5 °C above preindustrial levels. At the current pace, there is now a 50% probability of surpassing this threshold within nine years. Recent climate disasters, such as droughts, water crises, and wildfires, underscore the criticality of combatting global warming, irrespective of climate skeptics' opinions. The scientific community has established that one of the primary drivers of global warming is the rise in greenhouse gases, including carbon dioxide and methane. Since 1790, the onset of the industrial era, CO_2 emissions have soared by 50% (from 220 ppm to 447 ppm), coinciding with a corresponding 1.2 °C increase in temperature [1,2]. Halting the rise in atmospheric CO_2 levels is one of the most pressing environmental challenges of our time. In 2018, electricity generation remained the largest contributor to CO_2 emissions globally, accounting for 41% of total emissions from fossil fuel combustion, including natural gas, which is often touted as a cleaner burning alternative to coal [1]. This was followed by transportation at 25% and industry, which includes construction and cement manufacturing, at 18%. Capturing point sources of thermal power plant emissions (postcombustion) offers a viable strategy to mitigate the increase in anthropogenic CO_2 levels. However, flue gas streams generally exhibit a low concentration of CO_2 (3–15%, 0.03–0.15 bar) and are primarily composed of N_2 (75–80%, 0.75–0.80 bar), along with water (5–15%, 0.05–0.15 bar) and acid gases [3,4]. Therefore, the selective separation of CO_2 from other gases at a total pressure of 1 bar and a temperature range of 30–60 °C is essential. Currently, the most widely used method for post-combustion CO_2 capture involves the absorption of flue gas with an amine in the liquid phase, which effectively removes carbon dioxide. However, the regeneration process poses challenges due to the corrosive nature of the absorbents, resulting in high energy penalties and environmental concerns [5,6]. An alternative approach is physisorption using nanoporous materials like zeolites [7], silica [8], or activated carbons [9]. Adsorption-based separations, such as pressure-swing adsorption (PSA), are appealing due to their low energy requirements [10]. However, selecting an adsorbent with high CO_2 selectivity and capacity is crucial for PSA processes in CO_2 capture and separation. Physisorption criteria for optimal material selection include high CO_2 adsorption, high CO_2/N_2 selectivity in humid conditions, and low-energy cost desorption, consistent with a moderate heat of adsorption.

Over the past two decades, metal-organic frameworks (MOFs) have emerged as promising alternatives for CO_2 capture, owing to their high surface area and versatile chemistry. MOFs are two and three-dimensional crystalline porous coordination polymers, consisting of an inorganic moiety built from a metal ion connected to organic ligands [11–15]. They provide an optimal environment for post-combustion CO_2 capture and exhibit a reversible adsorption process that requires less regeneration energy than the amine processes [16]. It has been established over the past decade that the optimal physisorption characteristics for CO_2 capture from MOF materials [17] include CO_2 adsorption capacities at 0.15 bar

*aziz.ghoufi@univ-rennes1.fr

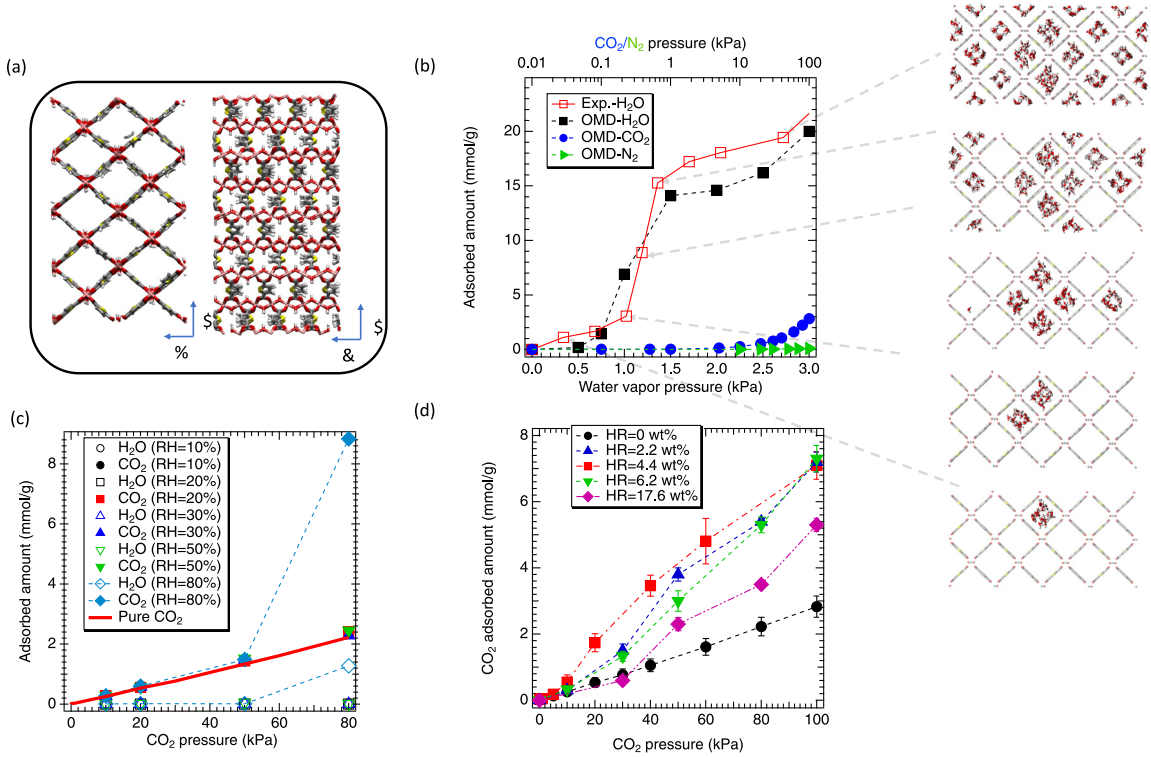

FIG. 1. (a) Illustration of the MIL-53-TDC MOF material along the *xz* and *yz* directions. (b) OMD-calculated water adsorption isotherm (bottom axis) and CO_2 and N_2 adsorption isotherms (top axis) within Al-MIL-53-TDC. Illustrations of confined water for different water vapor pressure values are shown on the right side. (c) OMD-simulated single and mixture CO_2/water isotherms with a relative humidity (RH) of 80%. (d) OMD-calculated CO_2 isotherms within Al-MIL-53-TDC as a function of different hydration rates (HR).

(CO_2 pressure in flue stream) greater than 1.5 $mmol \cdot g^{-1}$, high CO_2 affinity, less than 50 kJ mol^{-1}, and CO_2/N_2 selectivity greater than 30 [17–19]. Recently, Lin and coworkers developed a new MOF material, zinc-based Calgary Framework 20 (CALF-20), capable of physisorbing CO_2 with high capacity while also being selective over water [16,20] (1.9 mmol/g, CO_2 affinity ~38 kJ/mol, and a CO_2/N_2 selectivity of 75). As previously emphasized, CO_2 capture from MOFs must be studied in the presence of water, given its presence in the flue stream. This involves examining the structural stability of the MOF and ensuring the absence of deterioration of CO_2 adsorption capacity and CO_2/N_2 selectivity under humid conditions. One MOF material that has recently garnered attention for CO_2 capture is Al-MIL-53-TDC [21,22]. It is a Al-MIL-53 topology [23] constructed from 2,5-thiophenedicarboxylate (TDC) linkers and features chains of trans corner-sharing AlO_6 octahedra connected by linker molecules to create microporous, square-shaped 1D channels, as shown in Figs. 1(a) and 1(b). This MOF material exhibits high thermal stability, up to 420 °C in air, and permanent porosity toward N_2 and CO_2. It also boasts a high specific surface area of 1150 $m^2 \cdot g^{-1}$, a micropore volume of 0.48 $cm^3 \cdot g^{-1}$, and a CO_2 uptake of 2.1 mmol/g [24,25]. Recent kinetic uptake experiments conducted by Gonzalez-Martinez and colleagues revealed a 30% increase in CO_2 uptake (3 mmol/g) in the presence of water, which was attributed to the directionality of the hydrogen bond between water molecules and CO_2, as highlighted by first-principles calculations [24]. Although the authors highlighted a strong interaction between water molecules and hydroxide groups, no explicit correlation with the increase in adsorbed CO_2 uptake amount was provided, which means this phenomenon was not fully understood. However, other studies have also reported an enhancement in CO_2 adsorption amount [26,27], revealing that the interaction between the quadrupole moment of CO_2 and the electric field created by water molecules was responsible for the enhanced CO_2 uptake [26]. To sum up, water molecules act as additional interaction sites, creating a local electrical field that leads to an increase in CO_2 adsorption. However, although an increase in CO_2 uptake was evidenced from kinetic experiments with Al-MIL-53-TDC in the presence of water, no adsorption experiment was performed, and the effect of water on CO_2/N_2 selectivity was never studied. Furthermore, capillary condensation [28,29] was never considered to elucidate the enhanced CO_2 uptake in the presence of water in Al-MIL-53-TDC. The present work aims to use molecular simulations in the osmotic ensemble to predict and microscopically understand the adsorption isotherms of pure CO_2 and CO_2/N_2 mixtures within Al-MIL-53-TDC under humid conditions given the flexibility of Al-MIL-53-TDC [30].

II. COMPUTATIONAL METHOD

The simulation box consisted of 32 unit cells of Al-MIL-53-TDC arranged in the *x*, *y*, and *z* directions (2 × 4 × 4), and was constructed using the crystallographic coordinates reported in a previous study that combined x-ray powder diffraction (XRPD) and DFT calculations [22]. The

box dimensions are $L_x = 29.26$ Å, $L_y = 26.23$ Å, and $L_z = 58.90$ Å. Osmotic molecular dynamics (OMD) simulations were performed in the NσT ensemble, where N is the number of molecules, σ is the constraint and T is the temperature (303 K). Osmotic molecular dynamics simulations were employed to consider the flexibility of Al-MIL-53-TDC simultaneously with the adsorption process.

The developed OMD method is based on implementing a trial MC move for inserting/deleting a guest molecule during the MD trajectory in the osmotic ensemble [31–36]. The theoretical background for the OMD method is detailed in Refs. [31,36,37]. Both insertion and orientation bias are considered to improve the statistical sampling during the insertion/deletion move, and the insertion/deletion frequency can be adjusted with respect to the relaxation time of the system after the insertion/deletion of one molecule. A compromise must be found in terms of time and step intervals ($t_{ins/del}/N_{ins/del}$). As detailed in Ref. [36], to set up a more general approach that is system independent, the frequency of the insertion/deletion move is randomly chosen between 10 and 10 000 MD steps. Furthermore, in this OMD scheme, only one guest molecule is inserted/deleted, while a small time step of 0.5×10^{-4} ps is used to minimize the perturbation of the dynamics of the system. Regarding the thermostat and barostat, I opted for the Martyna-Tuckerman-Klein barostat [38] (MTK) algorithm, previously proven to allow sufficient pressure and thermal fluctuations [39]. Furthermore, the MTK integrator guarantees ergodic sampling. In this algorithm, the barostat relaxation time (τ_p) that controls the magnitude of the internal pressure and simulation box volume fluctuations was chosen to be $\tau_p = 0.5$ ps, while the thermostat relaxation time was taken to be 0.1 ps. OMD simulations were carried out by using a modified version of DLPOLY software [40], such that I implemented a Monte Carlo procedure in the main code. To calculate the adsorption isotherm, OMD simulations were performed for each gas pressure such that the final configuration obtained for gas pressure pi was the same as the initial configuration at p$i + 1$. Once the adsorbed amount was converged, additional MD simulations were carried out in the NσT ensemble, where σ is the constraint (1 bar), to calculate structural properties such as the radial distribution function. For each gas/vapor pressure, five OMD simulations were run with different empty Al-MIL-53-TDC by reinitializing the seed of the random number and using different processors to ensure the reproducibility of the obtained results.

The UFF [41] and DREIDING [42] force fields were combined to describe the flexibility of Al-MIL-53-TDC materials. UFF and DREIDING were used to describe the inorganic and organic moieties, respectively. This combination of two force fields treats the Al-MIL-53-TDC flexibility from bonding, bending, torsion, and improper intramolecular potential terms, while nonbonded interactions are described from Lennard-Jones (LJ) and electrostatic potentials. The UFF and DREIDING force fields are frequently employed in combination to characterize MOF materials. This amalgamation has demonstrated success in capturing MOF transitions and predicting adsorption isotherms for various gases [24,30,43–46]. Moreover, van der Waals interactions are encompassed through a 12-6 Lennard-Jones potential within both the UFF and DREIDING potentials, facilitating their integration. Notably, the MIL-53 MOF material has been commonly characterized using the UFF and DREIDING force fields in tandem. In line with the precedent set by previous force field developments, we adopted this combined approach. Following the procedure proposed by Chen *et al.*, the calculation of the partial charges of Al-MIL-53-TDC was carried out [47,48]. A combination of the Becke exchange plus the Lee-Yang-Parr correlation functional and all-electron core potentials was used. Additionally, the double-ζ numerical polarization (DNP) basis set was adopted to account for the d-type orbitals in heavier atoms and p-type polarization in hydrogen atoms. This basis is similar to the 6-31G(d, p) Gaussian-type basis set. The partial charges were calculated from the Mulliken population analysis using CASTEP [49]. Partial charges are reported in Fig. S1(a) of the Supplemental Material [50], and are similar to those reported by López-Olvera [22]. Water and CO_2 molecules were modeled by using the TIP4P/2005 [51] and EPM2 of Harris and Yung [52] models. Furthermore, the combined TIP4P/2005 and EPM2 models have been demonstrated to robustly reproduce thermodynamic and interfacial properties [53]. The water/CO_2/Al-MIL-53-TDC interactions were described by the LJ potential using the Lorentz Berthelot mixing rule [54,55]. All calculated interactions were truncated at a cutoff of 12 Å. Electrostatic interactions were modeled by means of the Ewald sum [56] using a relative error of 10^{-6} and a convergence parameter of 0.29 Å^{-1}. The simulated unit cell parameters are a = 15.68 Å, b = 7.31 Å, c = 13.76 Å, and $\beta = 90.3^\circ$ in fair concordance with the experiment [22], a = 14.63 Å, b = 6.56 Å, c = 14.73 Å, and $\beta = 90.0^\circ$. That corresponds to a variation of the unit cell volume of 10%, which validates the force field used. Furthermore, I report in Fig. S1(b) the pore size distribution (PSD) of the equilibrated configuration and that of the experimental structure [22]. As exhibited in Fig. S1(b), a fair agreement between both structures is obtained because a difference of 0.2 Å was found between both PSD maxima, which is an additional validation of the flexible force field. The difference between both profiles is the result of rotation of the thiophene-dicarboxylate rings ([Fig. S1(b)] that decreases the free accessible volume [57]. Recently, it was shown that the application of a mechanical pressure of 275 Mpa induced an irreversible structural transition toward a tightly closed phase with the following unit cell parameters: a = 19.236 Å, b = 8.478 Å, c = 6.674 Å, and $\beta = 111.06^\circ$ [30]. To validate the so-used force field, I applied a pressure of 200 Mpa to an equilibrated structure, and obtained the following unit cell parameters: a = 17.486 Å, b = 7.281 Å, c = 6.862 Å, and $\beta = 108.1^\circ$. The unit cell parameters are well reproduced, and the irreversibility is consistent with the fact that the relaxation of the closed form did not allow its reopening. Interestingly, the unit cell parameters obtained from the generic force field are found in fair agreement with experimental data (9% difference). Additional refinement will be needed to obtain a quantitative agreement [58]. However, our goal is not primarily quantitative; instead, it is to employ a generalized force field to comprehend a physical phenomenon. Snapshots of the open and closed structures are presented in Fig. S2(a) and Fig. S2(b), respectively. As shown in Fig. S2(b), a deformation of the cycle is highlighted, involving a slight shear in the x direction. This could be

attributed to backbone rotation and trampoline motion, as suggested for MIL-53 materials [59,60].

III. RESULTS

I initially investigated the adsorption of water to verify the Al-MIL-53-TDC material's ability to adsorb it. In Fig. 1(b), I present the water adsorption isotherm within Al-MIL-53-TDC. The isotherm aligns well with experimental data, confirming the precision of the model in describing H_20/Al-MIL-53-TDC molecular interactions. Between 1 kPa and 1.5 kPa, capillary condensation occurs, which is consistent with experimental data [24,25]. The water content fluctuates from 1 wt% to 9 wt% below 1 kPa, while beyond the capillary condensation, the water content reaches 27 wt%. Typically, flue gas streams contain 5–15 wt% water. Fig. 1(b) demonstrates that the Al-MIL-53-TDC MOF material gradually fills pore by pore with water, leading to local capillary condensation, until the channels are fully filled. In contrast, with CO_2 the channels are randomly and uniformly filled (see Fig. S3). CO_2 uptake is significantly lower than water uptake, suggesting that CO_2/MOF interactions are weaker than H_2O/water interactions. The isosteric heat of adsorption (QsT) for confined CO_2 and water are 18 kJ/mol and 33 kJ/mol, respectively, highlighting water's higher affinity with the Al-MIL-53-TDC framework.

In addition, I observed that unlike water, CO_2 fills all channels randomly and uniformly (see Fig. S3 of the Supplemental Material [50]). This is because water molecules (with a water-water interaction energy of 70.2 kJ/mol) have a higher affinity for the MOF surface (QsT = 33 kJ/mol) and begin to adsorb there, followed by clustering [with $E(H_2O/H_2O) = 70.2$ kJ/mol] until the channels reach full capacity (local capillary condensation). Figure S4(a) shows that the high energy of water-water interaction is due to hydrogen bonding between water molecules. QsT can be divided into two contributions: QsT(H_2O/H_2O) and QsT(Al-MIL-53-TDC/H_2O). The following values were obtained: QsT(H_2O/H_2O) = 22.3 kJ/mol and QsT(Al-MIL-53-TDC/H_2O) = 10.7 kJ/mol. In contrast, QsT(CO_2/CO_2) = 2.1 kJ/mol, and QsT(Al-MIL-53-TDC/CO_2) = 15.9 kJ/mol. These results confirm that water-water interactions are more favorable than MOF/adsorbate interactions and that water is also able to compete with CO_2 for adsorption sites in the Al-MIL-53-TDC material. To quantify this, I present in Fig. 1(c) the calculated binary CO_2/H_2O mixture adsorption isotherms for a range of relative humidity levels and total CO_2 pressures, ranging from 0 to 0.8 bar. As shown in this figure, CO_2 is slightly more preferentially adsorbed at low CO_2 pressures (0.1 bar), where $n_{CO_2} = 0.28$ mmol/g and $n_{H_2O} = 0.01$ mmol/g, corresponding to a CO_2/water selectivity of 84. This finding suggests that the Al-MIL-53-TDC MOF material is not particularly suitable for CO_2 capture, given its low CO_2 uptake (<1.5 mmol/g), despite exhibiting good CO_2/water selectivity.

Interestingly, at CO_2 pressures above 0.5 bar, I observe the adsorption of water molecules, resulting in a 320% increase in CO_2 uptake, from 2.1 mmol/g with no water to 8.8 mmol/g at 0.8 bar in the presence of H_2O, corresponding to a water uptake of 1.3 mmol/g (i.e., a hydration rate of 4.4 wt%). This clearly suggests that water molecules enhance CO_2 adsorption within Al-MIL-53-TDC. At low CO_2 pressure, I have observed that CO_2 is adsorbed in approximately the same quantity as in a single-case scenario. However, in the binary mixture, I have observed a slight reduction in water uptake in the presence of CO_2, as compared to the single water isotherm in Fig. 1(b). This finding highlights a competition between CO_2 and H_2O for different adsorption sites. Figure S4(b) in the Supplemental Material [50] shows that the radial distribution functions between oxygen atoms of water and CO_2 molecules with hydrogen atoms of hydroxide groups and sulfur atoms of Al-MIL-53-TDC have first peaks located at similar positions, around 4 Å beyond the distance of a favorable hydrogen bond interaction (2.5 Å). This indicates a lack of strong preferential adsorption sites (such as hydrogen bond sites) in Al-MIL-53-TDC. This finding is supported by the mean square displacement (MSD) shown in Fig. S5(a), where the MSD is linear and approximately 800 $Å^2$, corresponding to a displacement of 28 Å (which is the channel length), suggesting that water molecules are not anchored to specific MOF sites. Notably, the MSD of water molecules is about 10 times lower than that of CO_2 molecules, likely due to the high water density in the channel resulting from capillary condensation.

Based on these results, I decided to explore the impact of partially moisturizing of Al-MIL-53-TDC MOF material on CO_2 adsorption. Figure 1(d) shows the OMD-calculated CO_2 adsorption with varying hydration rates (HR) from 0 wt% to 17.6 wt%. The figure demonstrates a progressive increase in CO_2 uptake with the hydration rate, with the maximum value observed at an HR of 4.4 wt%, followed by a decrease for HRs ranging from 6.6 wt% to 17.6 wt%. An increase of 350% and 158% in CO_2 uptake is observed at 0.2 bar and 1 bar, respectively. To elucidate the molecular basis for the observed increase in CO_2 uptake in the presence of water, I analyzed the two-dimensional density profile of the center of mass of CO_2 molecules in the *xz* plane, as shown in Figs. 2(a) and 2(b). Figure 2(a) demonstrates that in the absence of water molecules, the channels of Al-MIL-53-TDC are equally sampled. In contrast, in the presence of water, channels are sampled heterogeneously, with high CO_2 density observed around the channels filled with water, as highlighted in Figs. 2(b) and 2(c). This is further supported by the two-dimensional profile of CO_2/water/Al-MIL-53-TDC energy reported in Fig. 2(d), where high-energy areas are located around the water pore, indicating additional water/CO_2 and Al-MIL-53-TDC/CO_2 interactions. These results suggest that the 2,5-thiophenedicarboxylate (TDC) linkers act as a permeable barrier highlighting the MOF's partial transparency to atomic interactions at the gas-solid interfaces. Transparency terms have been introduced to characterize the unique wetting transparency of graphene [61–63] involving that the van der Waals (vdW) interaction between graphene and any liquid placed on top of it is negligible, allowing the transmission of the substrate contact angle above graphene. In our case transparency is related to the transmission of water/CO_2 interactions through the organic linkers. The transparency to molecular interactions arises from the thinnest molecular walls, such as those found in graphene, boron nitride, or as shown in this work, the organic linkers. As stated by Koratar *et al.* in their work, graphene can partially transmit van der

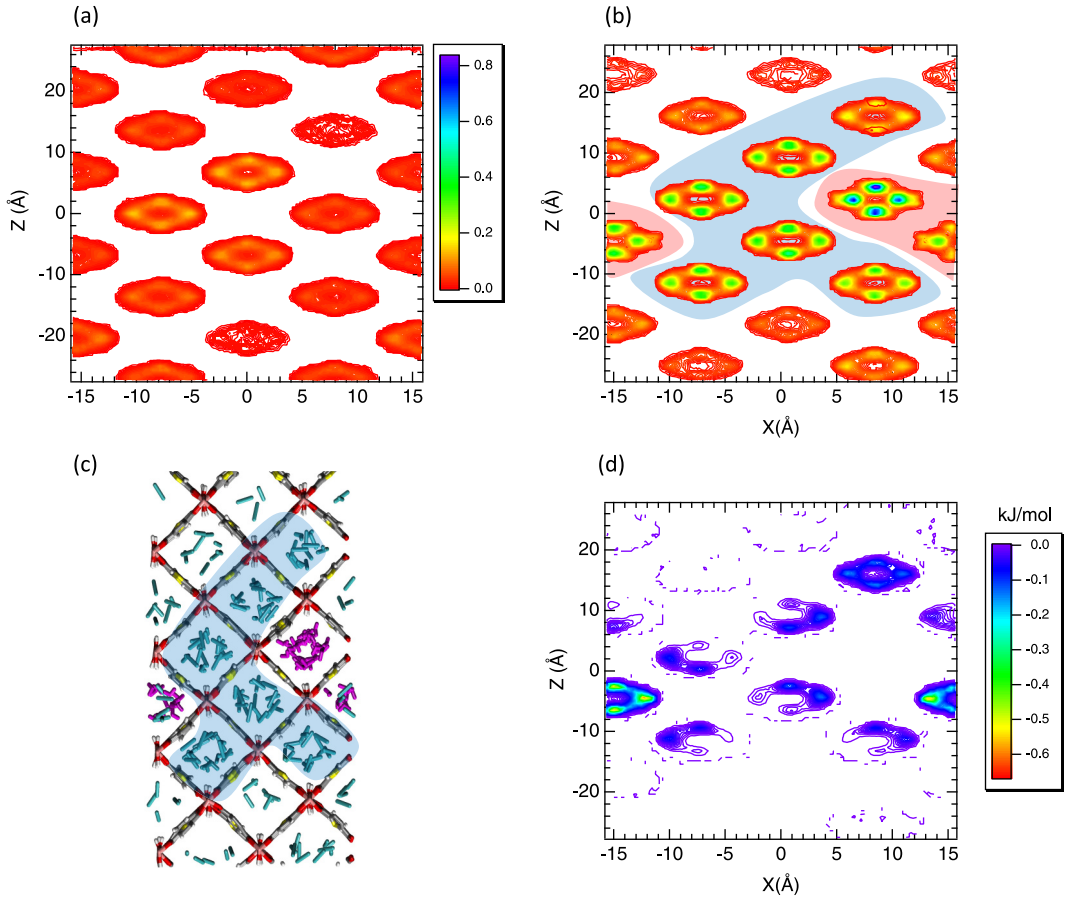

FIG. 2. Two-dimensional density profiles of the center of mass of CO_2 molecules in the *xz* direction are shown for single-component adsorption at a CO_2 pressure of 0.2 bar with (a) no water and (b) a HR of 4.4 wt% where the pink area corresponds to the water channels, while the blue region is connected to the channel with an increased amount of CO_2. (c) Snapshots of the filled MOF are shown for a HR of 4.4 wt% and a CO_2 pressure of 0.2 bar. The blue area corresponds to the channel with an increased amount of CO_2. (d) Two-dimensional *xz* free energy profile due to the CO_2/water interaction contributions.

Waals and electrostatic interactions between two media placed on either side of it [64,65]. Organic linkers possess a molecular size and can be attributed to this effect. Let's clarify that the term "transparency" also relates to an optical effect involving the passage of light through graphene, which isn't the focus of this particular work.

This transparency effect begins at low pressure, as depicted in Fig. S5(b), where an increase in CO_2 adsorption compared to the dry material is observed from a CO_2 pressure of 0.05 bar. Furthermore, Fig. S5(c) demonstrates that CO_2 molecules are adsorbed in channels surrounding the water pores due to the MOF's transparency, as soon as this pressure is reached. Furthermore, as hydrated pores do not adsorb CO_2 (few molecules), the increase in CO_2 uptake can only be attributed to interactions between water (H_2O) and CO_2 molecules occurring across the pores.

Interestingly, as shown in Fig. 1, the filling of metal-organic framework (MOF) channels is progressive and correlates with the pore capillary condensation that gives rise to the MOF's transparency. To study the role of the distribution of water molecules in the Al-MIL-53-TDC material, I randomly inserted water molecules to reach a relative humidity (RH) of 4.4 wt% and performed an equilibrium molecular dynamics simulation. After 10 nanoseconds, water clusters were formed, which is consistent with the first step of capillary condensation (local aggregation). The formation of small clusters was confirmed by calculating the cluster size distribution [Fig. S6(b)]. Figure S6(c) shows the calculated isotherm of CO_2 adsorption in the hydrated material (using both physical water distributions obtained from OMD simulation and random water filling) and the dry framework. As shown in Fig. S6(c), both fillings provide similar CO_2 isotherms, suggesting that the MOF's transparency effect can also develop from the water clusters localized in all pores.

Energetically, the heat of adsorption (QsT) was calculated as a function of CO_2 pressure and the adsorbed amount, and is reported in Fig. 3(a). The QsT calculation was based on total energy considerations. Figure 3(a) shows that the QsT of CO_2 confined in the hydrated MOF is 27% and 40% higher than the isosteric heat of adsorption in the case of unhydrated framework at 0.2 bar and 0.4 bar, respectively, which is consistent with previous energy calculations. The increase in QsT is attributed to the additional CO_2/water interactions resulting from the MOF's transparency. However, for a CO_2 pressure of 0.5 bar, the contribution of water/CO_2 interactions to QsT is only 11 kJ/mol, whereas the MOF/CO_2 contribution is 23 kJ/mol, indicating that additional interactions favor an increase in CO_2 uptake. I also

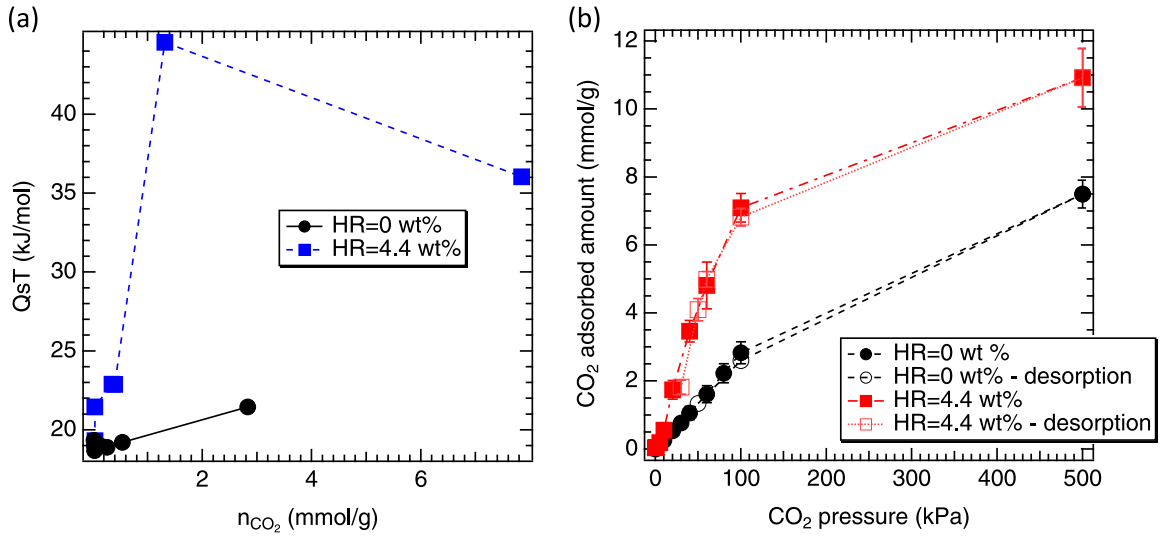

FIG. 3. (a) Isosteric heat of adsorption (Q_{ST}) as a function of the adsorbed CO_2 for both HR = 0 wt% and HR = 4.4 wt%. (b) Calculated CO_2 adsorption and desorption isotherms as a function of HR.

evaluated the QsT contribution of water/water interactions by considering the fluctuation of CO_2 molecules and quantifying their impact on confined water. Interestingly, the isosteric heat of adsorption of water/water interactions is 10.1 kJ/mol at a CO_2 pressure of 0.2 bar, which is of the same order of magnitude as the CO_2/water contribution (11 kJ/mol). This result may be due to the small amount of adsorbed CO_2 within the water pore. Figure S7 shows the water/water QsT [QsT(H_2O/H_2O)], the total hydrogen bond number (nHB), and the number of CO_2/H_2O pairwise interactions (n_{CO_2/H_2O}) separated by a distance smaller than 4.0 Å, which corresponds to the most probable distance obtained from the radial distribution function. The results indicate a correlation between QsT(H_2O/H_2O) and nHB, implying that the increase in QsT is due to the increase in n_{CO_2/H_2O} resulting from the rise in CO_2 concentration in the water nanopore. This leads to an increase in excluded volume for water molecules and truncation of the hydration shell of water, resulting in an increase in nHB [66–68], which favors the stability and structure of water/water interactions and is related to a kosmotropic effect. Figure S7 illustrates this relationship. Additionally, I present the adsorption/desorption branches of the CO_2 isotherm within the Al-MIL-53-TDC framework in Fig. 3(b). No hysteresis loop is observed for both the hydrated and dry MOF, indicating a fully reversible process.

I evaluated the MOF's transparency by examining the adsorption of CH_4 in both the hydrated and dry Al-MIL-53-TDC. As depicted in Fig. 4(a), the methane uptake is 33% lower than that of CO_2 (158–350%). Figure S8 illustrates that this is due to weaker host/CH_4 interactions, which are not as strong as host/CO_2 interactions. This is further supported by the QsT contribution related to water/guest interactions. The QsT contribution of water/CO_2 (977 J/mol) is higher than that of water/CH_4 (89 J/mol), indicating that stronger water/guest interactions lead to greater MOF transparency.

To better represent real flue gas streams, I calculated the OMD isotherm of CO_2/N_2 adsorption. As observed in Fig. 4(b), the selectivity of hydrated Al-MIL-53-TDC for CO_2/N_2 is increased by 185% and 204% at 0.2 bar and 0.8 bar, respectively, compared to the dry MOF. The selectivity values for CO_2/N_2 at 0.2 bar and 0.8 bar are 80 and 122, respectively. This increase is due to the CO_2 uptake increasing with the same magnitude as pure CO_2, while the amount of N_2 adsorbed is weakly impacted by the presence of water due to the combined weak N_2/H_2O and N_2/Al-MIL-53-TDC interactions, as shown in Fig. 4(c). The QsT of confined N_2 at low loading (0.3 mmol/g) is 4.3 kJ/mol, while the QsT of CO_2 within Al-MIL-53-TDC is 18.8 kJ/mol for a loading of 0.5 mmol/g. Finally, Fig. 4(d) shows the QsT of the N_2/CO_2 binary mixture as a function of CO_2 pressure for both hydrated and dry MOF. As shown, the total QsT in the hydrated MOF (45 kJ/mol) is greater than that in the dry state (19 kJ/mol) for a CO_2 pressure of 0.2 bar, as in the pure component, but still falls within the required range for industrial applications (<50 kJ/mol [18,19]).

IV. DISCUSSION

The preliminary findings indicate that the dry Al-MIL-53-TDC MOF material is not a viable candidate for CO_2 capture due to its low adsorption capacity (0.4 mmol/g) under a CO_2 pressure of 0.2 bar. However, the heat of adsorption, which was 18.6 kJ mol^{-1}, met the recommended QsT criterion of less than 50 kJ mol^{-1} [18,19]. Additionally, the N_2/CO_2 selectivity of 28 at a CO_2 pressure of 0.2 bar was marginally lower than the suggested selectivity of >30 [17].

However, by hydrating the Al-MIL-53-TDC MOF (from pore capillary condensation) at the hydration rate of 4.4 wt% it becomes a compelling adsorbent for CO_2 capture since a CO_2 adsorption capacity of 1.9 mmol/g, a QsT of 45 kJ/mol, and a selectivity of 80 at a CO_2 pressure of 0.2 bar were found. These improvements in CO_2 capture performance can be attributed to the MOF's capacity to transmit MOF/CO_2 and CO_2/CO_2 interactions. Indeed, the MOF material has uniaxial channels built with the thinnest molecular wall, allowing for transparency to van der Waals and electrostatic interactions. This permits the media on opposing sides of a molecular wall to perceive and impact each other.

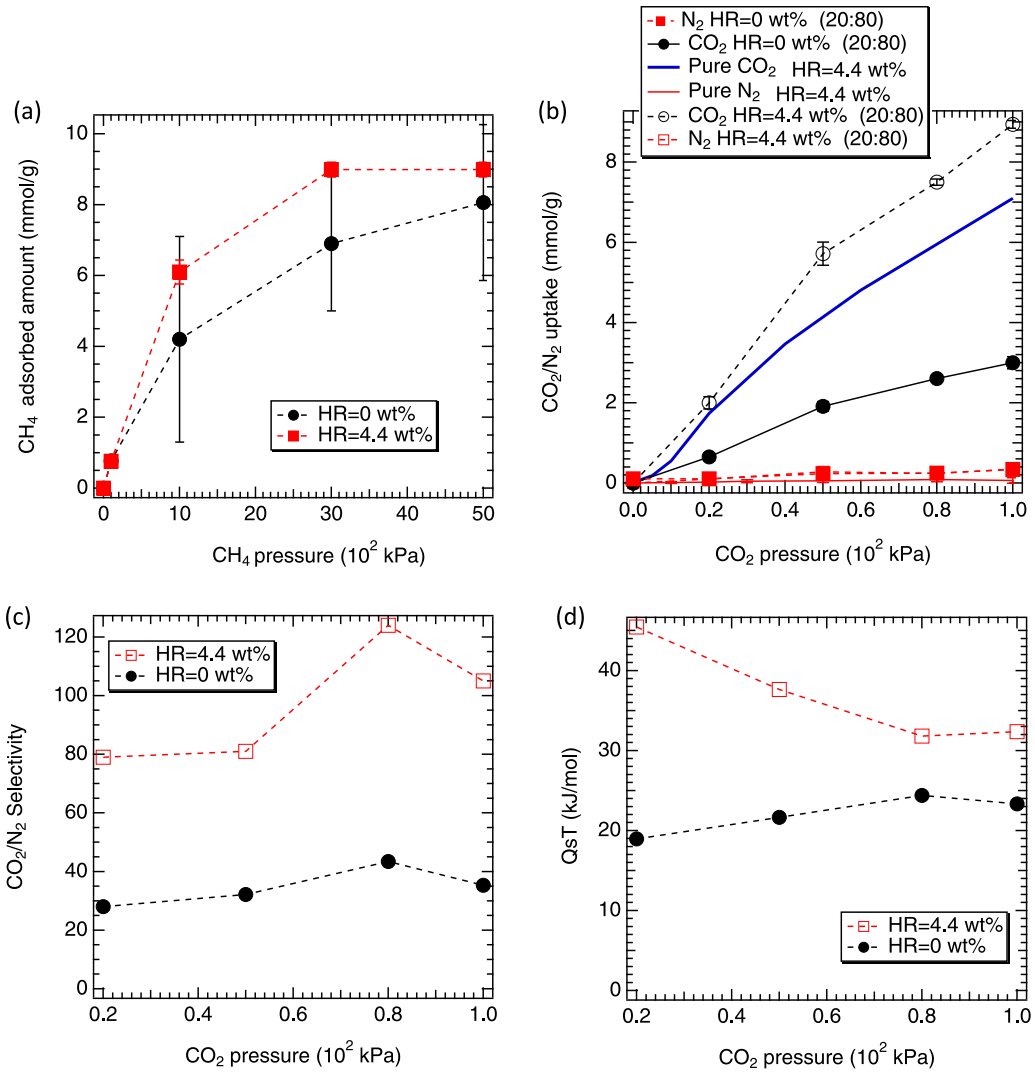

FIG. 4. (a) OMD-simulated methane isotherms as a function of both hydration rates, HR = 0 wt% and HR = 4.4 wt%. (b) Calculated single-component CO_2 and N_2, and binary CO_2/N_2 adsorption isotherms as a function of CO_2 pressure for both HR = 0 wt% and HR = 4.4 wt%. (c) Calculated CO_2/N_2 selectivity and (d) QsT for a mixture with a composition of 20:80 as a function of CO_2 pressure for two different HR values.

This study demonstrates that the optimal humidity level (4.4 wt%) results in the highest CO_2 adsorption. Moreover, I have highlighted that water adsorption is minimal up to 80% relative humidity. Therefore, there is no risk of water uptake increasing reducing CO_2 capture performance. It is noteworthy that CAU-10's CO_2 capacity decreases above an RH value of 20% [69], aluminum fumarate loses 17% CO_2 capacity at 14% RH, CALF-20 loses 100% CO_2 capacity at 80% RH [20], while Al-MIL-53-TDC maintains its high CO_2 capacity even at and above 80%. Additionally, I have confirmed that the initial humidity level (4.4 wt%) is unaffected during ternary water/CO_2/N_2 adsorption. Figure S9 shows a slight impact on initial water uptake.

These results provide a better understanding of how water enhances CO_2 uptake in porous materials with molecular walls separating uniaxial channels, revealing the transparency phenomenon. This knowledge could facilitate the potential reuse of old MOFs, such as MIL-47(V), with molecular walls between uniaxial channels. I then performed hydration of MIL-47(V) using the force field developed by Maurin *et al.* [70–72] and I calculated the CO_2 adsorption isotherms. Interestingly, I observed a slight effect on CO_2 sorption, indicating that the transparency effect is developing to a lesser extent in MIL-47(V) (an increase of 43% in CO_2 uptake at 0.8 bar). This is due to the nature of the organic ligand's aromatic cycle in MIL-47(V), which is constructed from a benzene ring with a well-aligned distance of 2.4 Å between hydrogen atoms of two neighboring cycles. In contrast, Al-MIL-53-TDC is built from a five-atom heterocycle (thiophene) with a distance of around 4.7 Å between sulfur and hydrogen atoms of two neighboring cycles [Figs. S10(a) and S10(b)]. This increased distance creates an opening between channels, leading to a more permeable wall that is responsible for the MOF's transparency. As shown in Fig. S10(c), interactions between water and CO_2 molecules can be developed between two channels. Ultimately, this finding could pave the way for the synthesis of new MOFs built from organic ligands containing five-atom heterocyclic

compounds such as furan, thiophene, pyrrole, or imidazole groups for CO_2 capture. To sum up, this study demonstrates the transparency of water interactions using the Al-MIL-53-TDC MOF material as an illustrative example. We extended our investigation to another MOF, MIL-47 (V), and concluded that specific conditions are required to observe a similar effect. Indeed, water molecules provide an additional attractive interaction that goes beyond the organic linkers, attracting CO_2 molecules from opposite sides of the organic linker. This results in an excluded volume for CO_2 molecules, which in turn leads to an increase in CO_2 uptake. This phenomenon occurs for specific ligands containing five-atom heterocyclic compounds creating an opening between channels, leading to a more permeable wall that benzenic cycles, what is responsible for the MOF's transparency. Finally, the transparency of MOFs is the result of a synergistic effect between water adsorption and presence specific organic ligands.

ACKNOWLEDGMENTS

I thank Nathalie Audebrand for fruitful discussions about structure of Al-MIL-53-TDC MOF material.

[1] M. Bui, C. S. Adjiman, A. Bardow, E. Anthony, A. Boston, S. Brown, P. Fennell, S. Fuss, A. Galindo, L. Hackett, J. P. Hallett, H. Herzog, G. Jackson, J. Kemper, S. Krevor, G. C. Maitland, M. Matuszewski, I. Metcalfe, C. Petit, G. Puxty *et al.*, Energy Environ. Sci. **11**, 1062 (2018).

[2] IPCC, Sixth assessment report of the intergovernmental panel on climate change (ipcc), 2022.

[3] T. Drage, C. Snape, L. Stevens, J. Wood, J. Wang, A. Cooper, R. Dawson, and X. Guo, in *Proceedings of the 3rd Gas Processing Symposium*, Vol. 3, edited by A. Aroussi and F. Benyahia Advances in Gas Processing (Elsevier, Oxford, 2012), pp. 30–37.

[4] R. E. James, D. Kearins, M. Turner, M. Woods, N. Kuehn, and A. Zoelle, Cost and performance baseline for fossil energy plants volume 1: Bituminous coal and natural gas to electricity. Report No.: NETL-PUB-22638.

[5] W. Gao, S. Liang, R. Wang, Q. jiang, Y. Zhang, Q. Zheng, B. Xie, C. Toe, X. Zhu, J. Wang, L. Huang, Y. Gao, Z. Wang, W. Jo, Q. Wang, L. Wang, Y. Liu, B. Louis, J. Scott, A.-C. Roger *et al.*, Chem. Soc. Rev. **49**, 8584 (2020).

[6] R. Siegelman, E. Kim, and J. Long, Nat. Mater. **20**, 1060 (2021).

[7] T.-H. Bae, M. Hudson, J. Mason, W. Queen, J. Dutton, K. Sumida, K. Micklash, S. Kaye, C. Brown, and J. Long, Energy Environ. Sci. **6**, 128 (2013).

[8] S. Pang, R. Lively, and C. Jones, ChemSusChem **11**, 2628 (2018).

[9] J. Mason, T. McDonald, T. Bae, J. Bachman, K. Sumida, J. Dutton, S. Kaye, and J. Long, J. Am. Chem. Soc. **137**, 4787 (2015).

[10] C. Voss, Adsorption **11**, 527 (2005).

[11] G. Ferey, Chem. Soc. Rev. **37**, 191 (2008).

[12] J. Li, S. J., and H. Zhou, Chem. Rev. **112**, 869 (2012).

[13] G. Férey, C. Serre, T. Devic, G. Maurin, H. Jobic, P. Llewellyn, G. D. Weireld, A. Vimont, M. Daturi, and J. Chang, Chem. Soc. Rev. **40**, 550 (2011).

[14] K. Sumida, D. L. Rogow, J. A. Mason, T. M. McDonald, E. D. Bloch, Z. R. Herm, T.-H. Bae, and J. R. Long, Chem. Rev. **112**, 724 (2012).

[15] M. Safaei, M. Foroughi, N. Ebrahimpoor, S. Jahani, A. Omidi, and M. Khatami, TrAC, Trends Anal. Chem. **118**, 401 (2019).

[16] J. Lin, T. Nguyen, R. Vaidhyanathan, J. Burner, J. Taylor, H. Durekova, F. Akhtar, R. K. Mah, O. Ghaffari-Nik, S. Marx, N. Fylstra, S. iremonger, K. Dawson, P. Sarkar, P. Hovington, A. Rajendran, T. Woo, and G. Shimizu, Science **374**, 1464 (2021).

[17] J. Kolle, M. Fayaz, and A. Sayari, Chem. Rev. **121**, 7280 (2021).

[18] L. Joss, M. Gazzani, and M. Mazzotti, Chem. Eng. Sci. **158**, 381 (2017).

[19] A. Gutierrez-Ortega, R. Nomen, J. Sempere, J. Parra, M. Montes-Moran, and R. Gonzales-Olmos, Chem. Eng. J. **435**, 134703 (2022).

[20] T. Nguyen, J. Lin, G. Shimizu, and A. Rajendran, Chem. Eng. J. **442**, 136263 (2022).

[21] P. Yot, L. Vanduyfhus, E. Alvarez, J. Rodriguez, J. Itié, P. Fabry, N. Guillou, T. Devic, I. Beurroies, P. Llewellyn, V. V. Speybroeck, C. Serre, and G. Maurin, Chem. Sci. **7**, 446 (2016).

[22] C. Tschense, N. Reimer, C.-W. Hsu, H. Reinsch, R. Siegel, W.-J. Chen, C. Lin, A. Cadiau, C. Serrre, J. Senker, and N. Stock, Z. Anorg. Allg. Chem. **643**, 1600 (2017).

[23] T. Loiseau, C. Serre, C. Huguenard, G. Fink, F. Taulelle, M. henry, T. Bataille, and G. Ferey, Chem. -A Eur. J. **10**, 1373 (2004).

[24] G. A. González-Martínez, T. Jurado-Vasquez, D. Solis-Ibarra, B. Vargas, E. Sanchez-Gonzalez, A. Martinez, R. Vargas, E. Gonzalez-Zamora, and I. Ibarra, Dalton Trans. **47**, 9459 (2018).

[25] A. López-Olvera, J. A. Zarate, E. Martinez-Ahumada, D. Fan, M. Diaz-Ramirez, P. Saenz-Cavazos, V. Martis, D. Williams, E. Sanchez-Gonzalez, G. Maurin, and I. Ibarra, ACS Appl. Mater. Interfaces **13**, 39363 (2021).

[26] A. Ö. Yazaydın, A. Benin, S. Faheem, P. Jakubczak, J. Low, R. Willis, and R. Snurr, Chem. Mater. **21**, 1425 (2009).

[27] Y. Magnin, E. Dirand, A. Orsikowsky, M. Plainchault, V. Pugnet, P. Cordier, and P. L. Llewellyn, J. Phys. Chem. C **126**, 3211 (2022).

[28] J. Canivet, J. Bonnefoy, C. Daniel, A. Legrand, B. Coasne, and D. Farrusseng, New J. Chem. **38**, 3102 (2014).

[29] K. C. Struckhoff, M. Thommes, and L. Sarkisov, Adv. Mater. Interfaces **7**, 2000184 (2020).

[30] M. Wahiduzzaman, N. Reimer, J.-P. Itie, N. Stock, G. Maurin, and P. Yot, Polyhedron **155**, 144 (2018).

[31] A. Ghoufi and G. Maurin, J. Phys. Chem. C **114**, 6496 (2010).

[32] F. Coudert, Phys. Chem. Chem. Phys. **12**, 10904 (2010).

[33] J. Zang, S. Nair, and D. Sholl, J. Chem. Phys. **134**, 184103 (2011).

[34] S. M. J. Rogge, R. Goeminne, R. Demuynck, J. J. Gutiérrez-Sevillano, S. Vandenbrande, L. Vanduyfhuys, M. Waroquier, T. Verstraelen, and V. Van Speybroeck, Adv. Theor. Simul. **2**, 1800177 (2019).

[35] Z. Yu, D. Anstine, S. E. Boulfelfel, C. Gu, C. Colina, and D. Sholl, ACS Appl. Mater. Interfaces **13**, 61305 (2021).

[36] H. Zhao, C. Pelgrin-Morvan, G. Maurin, and A. Ghoufi, Chem. Sci. **13**, 14336 (2022).
[37] H. Zhao, G. Maurin, and A. Ghoufi, J. Chem. Phys. **154**, 084702 (2021).
[38] G. Martyna, M. Tuckerman, D. Tobias, and M. Klein, Mol. Phys. **87**, 1117 (1996).
[39] S. Rogge, L. Vanduyfhuys, A. Ghysels, M. Waroquier, T. Verstraelen, G. Maurin, and V. V. Speybroeck, J. Chem. Theory Comput. **11**, 5583 (2015).
[40] T. Todorov, W. Smith, K. Trachenko, and M. T. Dove, J. Mater. Chem. **16**, 1911 (2006).
[41] A. K. Rappe, C. J. Casewit, K. S. Colwell, W. A. Goddard III, and W. M. Skiff, J. Am. Chem. Soc. **114**, 10024 (1992).
[42] S. L. Mayo, B. Olafson, and W. Goddard, J. Phys. Chem. **94**, 8897 (1990).
[43] L. Hamon, P. L. Llewellyn, T. Devic, A. Ghoufi, G. Clet, V. Guillerm, G. D. Pirngruber, G. Maurin, C. Serre, G. Driver, W. van Beek, E. Jolimatre, A. Vimont, M. Daturi, and G. Férey, J. Am. Chem. Soc. **131**, 17490 (2009).
[44] Q. Ma, Q. Yang, A. Ghoufi, G. Férey, C. Zhong, and G. Maurin, Dalton Trans. **41**, 3915 (2012).
[45] A. Ghoufi, A. Subercaze, Q. Ma, P. Yot, Y. Ke, I. Puente-Orench, T. Devic, V. Guillerm, C. Zhong, C. Serre, G. Ferey, and G. Maurin, J. Phys. Chem. C **116**, 13289 (2012).
[46] R. Renou, A. Szymczyk, G. Maurin, and A. Ghoufi, Mol. Sim. **41**, 483 (2015).
[47] F. Chen, R. Babarao, S. Sandler, and J. Jiang, Langmuir **26**, 8743 (2010).
[48] A. Ghoufi, J. Deschamps, and G. Maurin, J. Phys. Chem. C **116**, 10504 (2012).
[49] S. J. Clark, M. D. Segall, C. J. Pickard, P. J. Hasnip, M. J. Probert, K. Refson, and M. C. Payne, Z. Kristallogr. **220**, 567 (2005).
[50] See Supplemental Material http://link.aps.org/supplemental/10.1103/PhysRevMaterials.7.126001 for additional Figs. S1– S10 and partial charge on MOF structure, and a table providing unit cell parameters. The Supplemental Material also contains Refs. [21,22].
[51] J. Abascal and C. Vega, J. Chem. Phys. **123**, 234505 (2005).
[52] J. Harris and K. Yung, J. Phys. Chem. **99**, 12021 (1995).
[53] A. Ghoufi, F. Goujon, V. Lachet, and P. Malfreyt, J. Chem. Phys. **128**, 154716 (2008).
[54] H. A. Lorentz, Ann. Phys. **248**, 127 (1881).
[55] D. Berthelot, C. R. Hebd. Seances Acad. Sci. **126**, 1703 (1898).
[56] P. P. Ewald, Ann. Phys. **369**, 253 (1921).
[57] The Input/output OMD files are available on the GitHub platform, https://github.com/aghoufi/MIL-53-NH2.
[58] F. Salles, A. Ghoufi, G.Maurin, R. Bell, C. Mellot-Draznieks, P. Llewellyn, C. Serre, and G. Ferey, Angew. Chem. Int. Ed. **47**, 8487 (2008).
[59] J. Mowat, V. Seymour, J. Griffin, S. Thompson, A. Slawin, D. Fairen-Jimenez, T. Duren, S. Ashbrook, and P. Wright, Dalton Trans. **41**, 3937 (2012).
[60] A. Hoffman, J. Wieme, S. Rogge, L. Vanduyfhuys, and V. V. Speybroeck, Z. Kristallogr. **234**, 529 (2019).
[61] J. Rafiee, X. Mi, H. Gullapalli, A. Thomas, F. Yavari, Y. Shi, P. Ajayan, and N. Koratkar, Nat. Mater. **11**, 217 (2012).
[62] C.-J. Shih, M. Strano, and D. Blankschtein, Nat. Mater. **12**, 866 (2013).
[63] C.-J. Shih, Q. H. Wang, S. Lin, K.-C. Park, Z. Jin, M. S. Strano, and D. Blankschtein, Phys. Rev. Lett. **115**, 049901(E) (2015).
[64] D. Ghoshal, R. Jain, and N. A. Koratkar, Langmuir **35**, 12306 (2019).
[65] F. Presel, A. Gijon, E. R. Hernandez, P. Lacovig, S. Lizzit, D. Alfe, and A. Baraldi, ACS Nano **13**, 12230 (2019).
[66] A. Ghoufi, I. Hureau, D. Morineau, R. Renou, and A. Szymczyk, J. Phys. Chem. C **117**, 15203 (2013).
[67] R. Renou, A. Ghoufi, A. Szymczyk, H. Zhu, J.-C. Neyt, and P. Malfreyt, J. Phys. Chem. C **117**, 11017 (2013).
[68] R. Renou, A. Szymczyk, and A. Ghoufi, J. Chem. Phys. **140**, 044704 (2014).
[69] V. B. Lopez-Cervantes, E. Sanchez-Gonzalez, T. Jurado-Vasquez, A. Tejeda-Cruz, E. Gonzalez-Zamora, and I. A. Ibarra, Polyhedron **155**, 163 (2018).
[70] H. Jobic, N. Rosenbach, Jr., A. Ghoufi, D. Kolokov, P. Yot, T. Devic, C. Serre, G. Ferey, and G. Maurin, Chem. -A Eur. J. **16**, 10337 (2010).
[71] P. Yot, Q. Ma, J. Haines, Q. Yang, A. Ghoufi, T. Devic, C. Serre, V. Dimitriev, G. Ferey, C. Zhong, and G. Maurin, Chem. Sci. **3**, 1100 (2012).
[72] P. Llewellyn, S. Bourrelly, C. Vagner, N. Heymans, H. Leclerc, A. ghoufi, P. Bazin, A. Vimont, M. Daturi, T. Devic, C. Serre, G. D. Weirel, and G. Maurin, J. Phys. Chem. C **117**, 962 (2013).